International Journal of Rock Mechanics & Mining Sciences 81 (2016) 1–11

Contents lists available at ScienceDirect

International Journal of Rock Mechanics & Mining Sciences

journal homepage: www.elsevier.com/locate/ijrmms

Technical Note

Quantifying rock mass bulking at a deep underground nickel mine

C. Groccia [a,b], M. Cai [a,b,*], A. Punkkinen [c]

[a] Geomechanics Research Centre, MIRARCO, Laurentian University, Sudbury, Ont., Canada P3E 2C6
[b] Bharti School of Engineering, Laurentian University, Sudbury, Ont., Canada
[c] Creighton Mine, Vale Ltd., Sudbury, Ont., Canada

ARTICLE INFO

Article history:
Received 20 May 2014
Received in revised form
27 March 2015
Accepted 4 June 2015

Keywords:
Rock mass bulking
Brittle failure
Depth of failure
Field measurements
Creighton Mine

1. Introduction

In deep underground mining and construction, high stress-induced rock fracturing is inevitable.[1] Rock near the boundary of an excavation is confined in the tangential direction, and the volume increase due to rock failure is often translated into a significant convergence of the excavation boundary, and this phenomenon is known as rock mass bulking.[2] Fig. 1 shows how the periphery of an excavation can deform from the original shape (shown as a dashed line) to a new shape (shown as the solid interior line), as a result of an increase in volume of the shaded failed zone. Rock mass bulking can cause problems when the wall displacement exceeds the displacement capacity of the support elements.[3,4] In extreme cases the wall deformation can be very large, reducing the effective span of the drift and making the drift unsuitable for mining access. Thus, it is important to predict and manage rock mass bulking when mining in highly stressed grounds.

The amount of convergence that can be expected due to rock mass bulking can be predicted by multiplying a Bulking Factor (BF) by the expected depth of failure. The relationship between the bulking factor and the total wall convergence (U_w), the convergence due to elastic deformation at the boundary of the non-failed and failed zones (U_{df}), and the depth of failure (d_f) is:

$$BF = \frac{U_w - U_{df}}{d_f} \tag{1}$$

Compared with U_w, the amount of deformation of U_{df} is small; therefore, the wall convergence can be approximated by

$$U_w \approx BF \times d_f \tag{2}$$

Current empirical methods for predicting bulking factors are based on limited, often qualitative data because there are few case studies where the necessary parameters have been collected or documented. In order to back calculate a bulking factor, the depth of failure and the convergence of the surface of the excavation must be measured. Measuring U_{df} is not crucial because it can be predicted using conventional continuum numerical modeling techniques. This amount of deformation is small relative to wall convergence due to rock mass bulking and as such will have a negligible effect on the back calculation of the bulking factor.

The data included in previous case studies used to back calculate bulking factors[5] were usually not collected with similar objectives. For the purpose of this study, there was an obvious lack of information on the depth of failure in these datasets. Case studies with extensometer data from Kloof Gold Mine[6] and the Donkin-Morien Tunnel[7] are more useful because the convergence was directly measured and the depth of failure can be inferred from the measurement from the point where the convergence transitions from linear (elastic deformation) to nonlinear (plastic deformation/bulking). Limitations associated with the use of extensometers are their limited deformation coverage range, limited resolution that is dependent on the spacing of the measurement points, and high cost when installation at multiple locations

* Corresponding author at: Geomechanics Research Centre, MIRARCO, Laurentian University, Sudbury, Ont., Canada P3E 2C6.
E-mail address: mcai@laurentian.ca (M. Cai).

http://dx.doi.org/10.1016/j.ijrmms.2015.06.014
1365-1609/

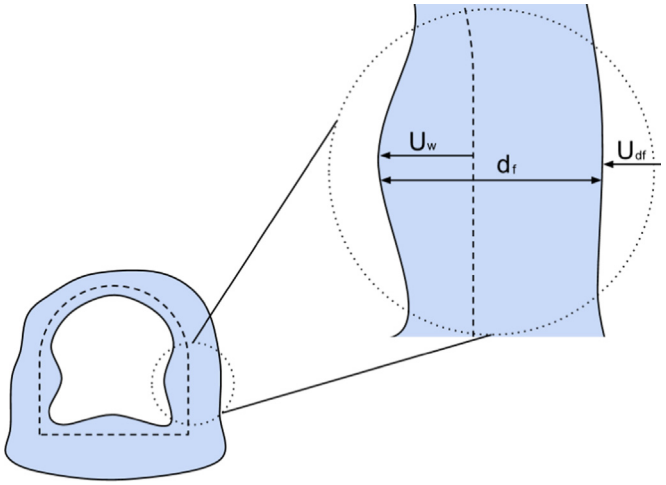

Fig. 1. Concept of rock mass bulking (based on Ref. 2).

around the periphery of an excavation is required.

The need for case studies focusing on rock mass bulking is apparent to researchers and engineers working to advance methods of modeling or predicting rock mass bulking. The objectives of this study were to collect quantitative bulking measurements and to study factors that influence rock mass bulking at Creighton Mine in Sudbury, Ontario, Canada. Various data collection techniques have been used to ensure that the site monitoring is as complete as possible, and the merits of the techniques can be judged for future rock mass bulking observations.

2. Geological setting and description of the observation site

2.1. Geological setting

Creighton Mine, which is owned and operated by Vale, is a deep underground nickel mine located in the Sudbury Basin. The mine has been in continuous production for more than a century with current active mining levels at depths of 2.3–2.5 km. The mine is seismically active[8] and managing seismic risk and controlling rockburst damage are challenging tasks facing the mine as mining progresses to deeper levels.

Creighton Mine is located in the southeast corner of an embayment of a nickel irruptive into the footwall rocks. In general, the lower norite member of the main irruptive is the hangingwall of the orebody. The footwall rocks are metavolcanics of the Elsie Mountain Formation, Lower Huronian in age and intruded by granite/gabbros. The orebody (OB) at depth is generally steeply dipping within high grade massive and inclusion massive sulfides adjacent to the barren granites and gabbros and a gradational lower grade hangingwall zone. Structurally controlled, the orebody has gradually shifted into two distinct production areas below the 2340 m production level. Massive and inclusion massive sulphides are high grade and copper rich, considerable shearing and quartz veining exists throughout the third production front at depth. Quartz veining and shearing, often infilled with quartz carbonate, is typically inter-connected through the footwall rocks by a family of distinct splays, influencing how mining-induced stresses are redistributed and contribute to mine seismicity.

2.2. Observation site

An observation site for the project (Fig. 2) was set up in a newly developed drift in the mine at a depth of approximately 2.4 km from the surface. This site was selected because it was situated at a location that was already under high stress due to the overburden depth and proximity to the orebody. This location was expected to undergo an increase in mining-induced stress with the excavation of nearby stopes as the stresses are further redistributed. The purpose of establishing the observation site was to quantitatively monitor the development of stress-induced damage around the drift and the associated rock mass bulking as a result of the damage.

Eleven BQ size diamond drill holes (DDH) were drilled in an array around the excavation (Fig. 3). Diamond drilling provided key advantages because it allowed for core logging and testing in the lab and resulted in a smooth inner surface for quality observation of the holes. A smooth inner surface of the observation holes greatly improves the quality of data that can be retrieved using various down-the-hole probes. Six pairs of reference points marking vertical cross-sections were used for subsequent convergence monitoring (Fig. 2). Following drilling of the holes, a safety bay was excavated at a later stage, changing the profile of the drift where the observation holes were located. The safety bay was used to observe the rock mass condition of the drift wall itself by providing a cross-sectional view of stress-induced surface parallel fracturing. The DDH holes were used to monitor the depth of stress-induced fracturing using a variety of tools and the reference points were used to align recurring vertical cross-sections

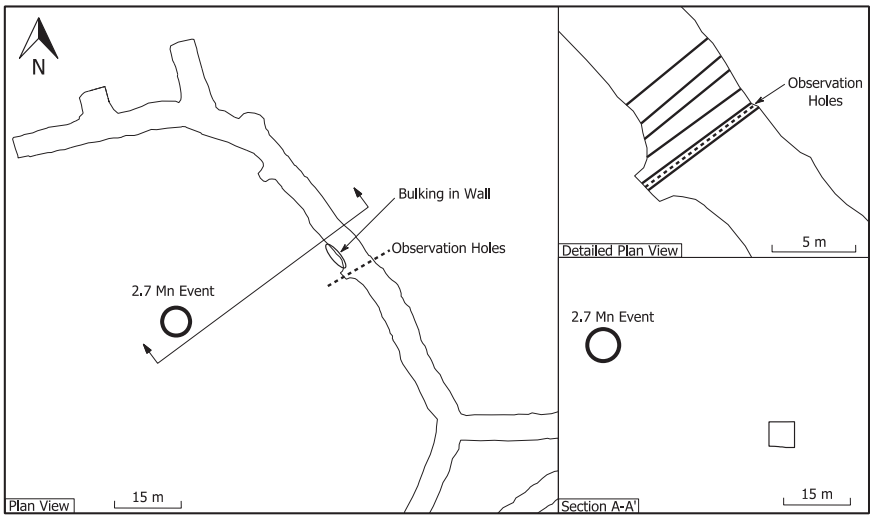

Fig. 2. Locations of observational cross-sections at the observation site and the position of the 2.7 M_n seismic event.

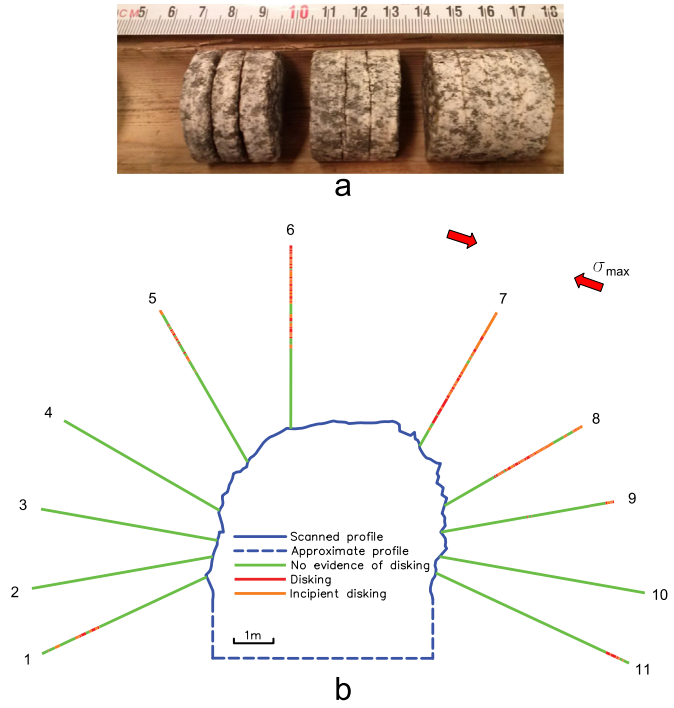

Fig. 3. (a) Examples of disking (left), and varying degrees of incipient disking (center and right). (b) Location of core disking and incipient core disking in cores from boreholes at the observation site.

that were scanned by a laser scanner during each site visit. Cross-sections 1 and 2 (CS1 and CS2) were parallel to the plane in which the 11 observation holes were drilled and located 25 cm to either side of the plane. The sections were oriented in this fashion to prevent scanning on the exact plane that the observation holes were drilled and avoiding laser scan readings from the inside of any drill hole, which would not be representative of the location of the excavation surface.

2.3. Geotechnical conditions

Core from the holes drilled at the observation site was used to characterize the immediately surrounding rock mass. Using the modified Tunnel Quality Index based on the Q system[9], the Q' index value was determined to be 111 (Very Good to Extremely Good rock), which corresponded to a Geological Strength Index (GSI)[10] of 86. Laboratory tests were conducted at the MIRARCO's Geomechanics Research Centre Laboratory. The uniaxial compressive strengths of most rock samples were between 150 and 300 MPa, with an average of about 180 MPa. Because the test samples were taken from the observation holes in stressed ground near the excavation, a certain degree of sample damage was inevitable.[11] Hence, the actual in-situ rock strength may be higher than the values tested in the laboratory.

2.4. 2.7 M_n seismic event

On April 15th, 2013, a seismic event with a magnitude of 2.7 M_n (Nuttli) occurred at the mine and resulted in minor damage to the observation site. The source location of the seismic event, which is approximately 45 m from the observation site, is shown in Fig. 2. Geotechnical staff at the mine site reported that within the vicinity of the observation site the floor heaved adjacent to bulking in the west wall, two 20 mm rebar bolts used to secure ventilation ducting in the back failed at the threads, and one 46 mm friction bolt (Split set) installed in the wall failed at the point where the ring was welded on to the end of the bolt. Rock mass bulking was well retained by the rock support system installed utilizing 46 mm friction sets and #4 gauge galvanized mesh. This seismic event occurred during the monitoring period of this project and the seismic source was close enough to the observation site to initiate damage in the observation holes and resulted in changes in the measured cross-sectional profiles. Measurements were collected before and after the damage occurred for subsequent analysis.

2.5. Core disking

Recovered cores from the observation holes provided a closer look at the rock and joint surface conditions, which would not have been possible using only in-the-hole methods. The cores were logged for joint properties, discontinuity locations, lithology, and the occurrence of disking and partial or incipient disking. A distinction was made between disking and incipient disking. Disking resulted in complete separation of the disks whereas incipient disking only caused damage to the core with disks remaining bonded together. Fig. 3a presents examples of disking and varying degrees of incipient disking from the core.

Fig. 3b presents the locations where disking and incipient disking occurred in the cores. Because there is no distinguishable change in rock properties where the core damage begins and ends, it can be assumed that the core damage indicates that the stress was higher in the areas where disking and incipient disking occurred than in areas where no disking occurred. Core disking data can be used to infer stress magnitudes and orientations[12,13]; however, published trends would need to be verified at this particular site before this information could be used with any confidence to infer the stress magnitudes. Based on the locations of the observed disking and incipient disking, it can be inferred that the orientation of the maximum principal stress in the observed plane is roughly perpendicular to Hole 7 as shown in Fig. 3b.

The scanned profile of the drift shown in Fig. 3b is CS1, which was captured when the observation holes were drilled. At this time, the drift face had advanced a few drift diameters ahead of the observation holes shown in Fig. 2. The core disking is representative of the drift profile and stress conditions when the holes were drilled; thus, only the original drift profile is used when considering the occurrence of disking. Under elastic conditions, the highest stress will occur at the excavation boundary, tangential to the boundary of the excavation and parallel to the maximum principal stress direction. As can be seen in Fig. 3b, the rock mass has undergone some inelastic deformation upon excavation, leading to a stress relaxation zone surrounding the excavation. As a result, disking did not occur at the excavation boundary in Holes 6–8 as would otherwise be expected.

3. Laser scanning

Measuring the convergence of the surface of an excavation is required to quantify rock mass bulking. A Leica 3D Disto laser scanner was used to scan vertical cross-sections at the observation site. Fig. 4b presents scans of CS6 taken on December 4th, 2012 and April 17th, 2013. The scan clearly shows that the deepest overbreak is in the same region as where core disking was most prevalent. The overbreak and core disking are indicators of high stress and they both show similar direction of the maximum principal stress in the plane of the cross-section, i.e., perpendicular to the breakout and the borehole with the most extensive core disking. The notch likely developed due to the redistribution of stresses when the excavation round of the drift was blasted, and progressed during the scaling and bolting process during installation of the rock support. There were no signs of further notch

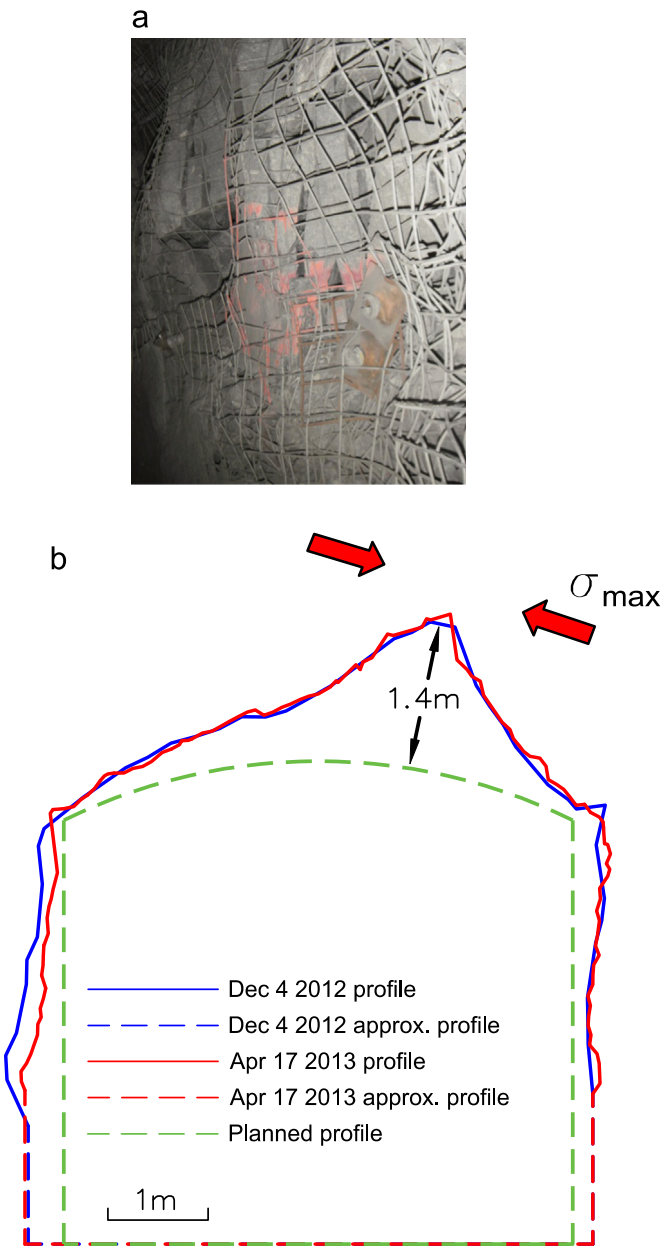

Fig. 4. (a) Photo of rock mass bulking looking south and (b) scans of a cross-section 5 m from the array of observation holes that show up to 200 mm of convergence.

progression once the rock support was installed. This highlights the importance of installing support quickly after blasting and shows that the support system is very effective in preventing further failure of the rock mass.

When the observation site was rescanned after the 2.7 M_n seismic event occurred on April 15th, 2013, it was discovered that there had been no obvious deformation in the cross-sections alongside the observation holes (CS1 and CS2 in Fig. 2), but significant deformation had occurred in the wall approximately 4–5 m from the observation holes at CS5 and CS6.

Fig. 4a shows the fractured rocks on the wall at CS6, retained by #4 gauge welded wire mesh and 46 mm friction sets. The convergence that occurred as a result of the damage can be easily quantified by comparing laser scans of the cross-section before and after the damaging seismic event. Up to 200 mm of convergence was recorded on the left-hand side wall using the scans shown in Fig. 4b. However, it should be noted that the effect of the nearby safety bay may have contributed to some of the convergence following the seismic event due to a geometrical effect that may result in a reduction in confinement of the rock mass in the adjacent wall.

4. Measuring the fractured zone

Empirical methods[2,14] have been developed to estimate the depth of failure surrounding an excavation. The depth of failure depends on many factors such as stress magnitudes and orientations, rock mass strength, excavation shape, and most importantly the installed rock support. The empirical methods provide a good estimate when there is no rock support or the installed rock support is not effective. Whenever possible, direct measurement of the depth of failure is recommended.

Measuring the depth of the fractured zone is required to quantify rock mass bulking; however, there is no established best practice for performing the work. For this reason, a number of methods such as core photograph examination, borehole camera logging, core logging, optical televiewer logging, and ultrasonic velocity logging were investigated to determine the best approach for this purpose.

4.1. Core and optical televiewer logging

An OBI40 optical televiewer by Advanced Logic Technology was used to log the observation holes to identify the location of fractures that intersect the holes. The televiewer acquires a 360 degree image of the wall of a hole at pre-defined depth intervals. The image from each depth interval is unwrapped to create a narrow strip of pixels that is one pixel tall with the width depending on the azimuthal resolution. All of the acquired strips of pixels are stacked to create an image with known depths. This is a very accurate way of measuring the location of features that intersect holes. Furthermore, televiewer images provide not only the location but also the orientation and aperture of fractures, which are useful for rock mass characterization. Another advantage of using televiewer images is that all of the fractures seen in the image are actual in-situ fractures, which means that they are either pre-existing or mining-induced fractures, as opposed to drilling-induced fractures that may exist in the core which could be mislabeled.

The bottom part of Fig. 5 is a televiewer image captured from the first meter of Hole 7 with a picture of the core from the same

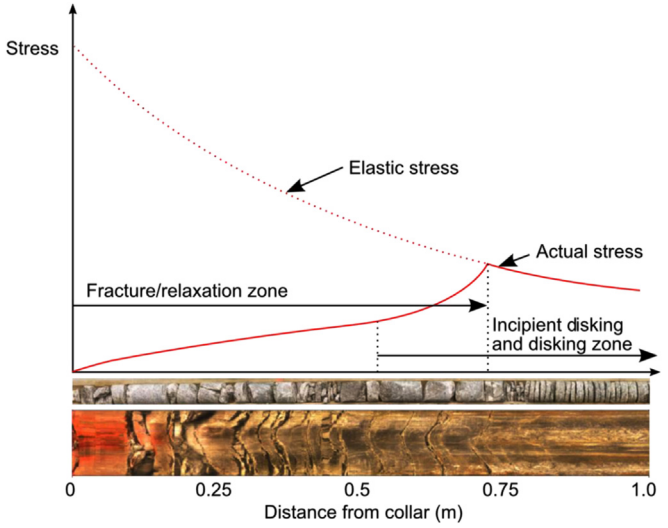

Fig. 5. Photograph of core on top of the corresponding televiewer image from the first meter of Hole 7.

section shown above. When viewing the two images side-by-side, it becomes obvious that determining the exact depth of the fractured zone from viewing the cores alone is not possible when the cores are broken to a point where they cannot be perfectly reassembled. In this case, the televiewer log is a more useful method of accurately determining the depth of failure and the core log provides insights regarding the stress conditions when the holes were drilled.

The deepest open fracture in the televiewer image is located slightly more than 0.7 m from the collar of the hole (Fig. 5). It is at this point that disking begins to appear in the core, indicating that the rock before this point has undergone some stress relaxation due to rock fracturing. However, there is incipient disking in the core piece located between 0.55 and 0.6 m, which indicates that while there might have been some stress relaxation due to fracturing, the stress was still relatively high at this point when the borehole was drilled. The graph at the top is an interpretation of the tangential stress along Hole 7 based on observations from the core and televiewer images. As can be seen in the graph, the actual stress state deviates from the elastic stress state significantly and there is an overlapping of the fractured/relaxed zones and the disking/incipient disking zones. A combination of televiewer and core logging data allows the depth of failure to be determined more objectively. For this case, the depth of failure in Hole 7 can be assessed as 0.7 m based on the information collected.

Based on the combined information provided by televiewer and core logging, we can see that it is possible to make an estimate of the depth of the fractured zone based on the core log, i.e., the depth of fractured zone can be defined by the location where disking starts. From Fig. 5, we can see that the estimated depth would be about 0.75 m in Hole 7. This is based on the observation that disking in the core can only happen when the ground stress is sufficiently high. If there is no stress fracturing in the shallow section of the borehole, disking should appear starting from the collar where the tangential stress is the highest. If the rock is fractured in-situ, the stress will be relaxed and disking in the core will not occur when the drill bit passes the stress-relaxed rocks. This insight was obtained based on the core log and the televiewer log shown in Fig. 5. One example that supports this conclusion is shown in Fig. 6. The cross-section of Room 418-U1 array at the Underground Research Laboratory (URL) in Canada is shown in Fig. 6b with core disking information presented [12]. There was no stress-induced rock fracturing at this tunnel site (Fig. 6a), and the drilling-induced disking started right from the boundary of the tunnel (Fig. 6b) where the tangential stress was the highest.

Using the same method, the depth of failure in Holes 5, 6, and 8 can be estimated and the results are shown in Figs. 3 and 8. The depths of failure determined from the core disking method and the televiewer logging method are consistent in Holes 6, 7, 8; however, a large difference is seen in Hole 5. The angles of the maximum field stress with Holes 6–8 are large but small in Hole 5. This could be the reason why the core disking method provides an unreliable estimate of the depth of failure in Hole 5. Hence, the core method is likely only valid when disking is present in the cores and when the maximum principal stress is intercepting the hole at a large angle. Disking occurs in Holes 1, 9, and 11, at locations far away from the collars. The spot disking was likely induced by local stress concentration caused by rock heterogeneity. In addition, these holes intercept with the maximum principal stress at smaller angles and the core disking method for depth of failure estimation is not applicable to these holes.

Fig. 7 shows a side-by-side comparison of the core photo and two televiewer images of the first meter of Hole 3, measured from the collar (refer to Fig. 3 for the hole location). No core disking occurred in this hole because the maximum field stress is almost parallel to the hole and the hole is shadowed from the maximum

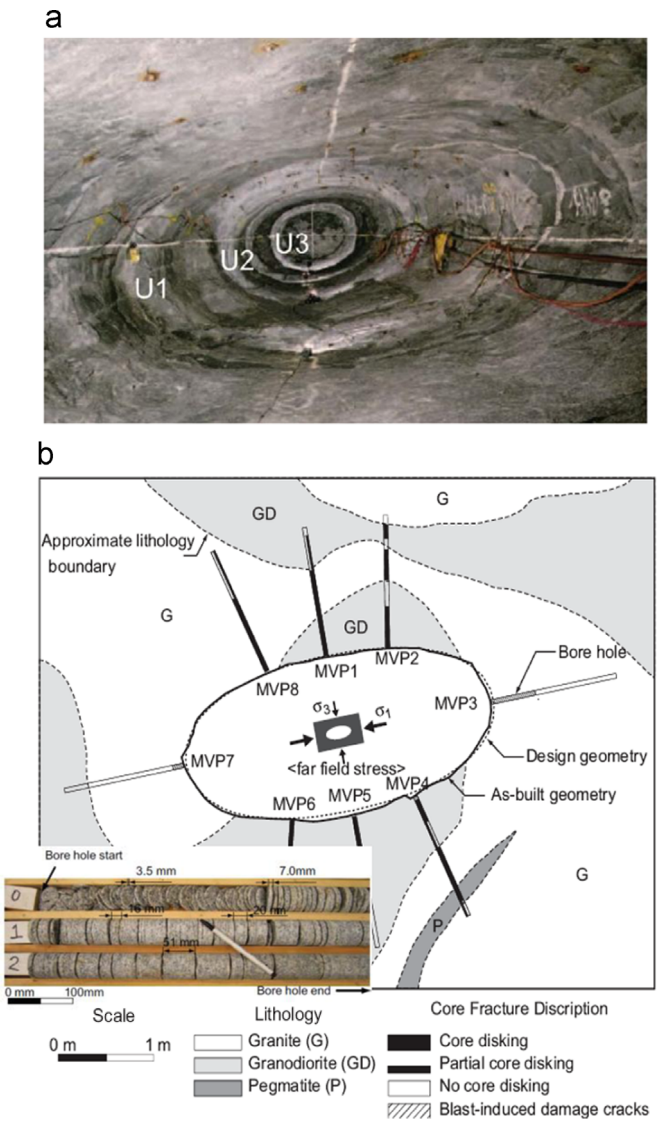

Fig. 6. (a) Photo of Room 418 showing the room geometry at U1, -U2 and -U3 cross-sections; (b) cross-section of Room 418-U1 array showing the MPV boreholes and core disking status; insert: typical core disking from a MVP borehole[12].

principal stress induced by the excavation. In this situation, the depth of failure can only be assessed using the televiewer image. From the time when the first logging was completed (November 20, 2012) to the time when the second logging was completed (May 7, 2013), some new fractures developed and some existing fractures opened slightly. The fracture located at approximately 0.2 m from the collar is a new fracture, and the fractures located at 0.1 m and 0.25 m are existing fractures that have opened up. A small wedge fell out of the hole wall at approximately 0.5 m and there were some indications of damage between 0.5 and 0.75 m which is believed to be due to blasting when the safety bay was excavated. It can be difficult to discern these features from examining a JPEG image like the one shown in Fig. 7, but they are better visualized using software such as “WellCAD”, which was used to process the televiewer images. The software offers enhanced visualization capability and maintains a higher image quality, making it easier to notice changes in fracture number and aperture.

Side-by-side comparisons like the one shown in Fig. 7 were used to interpret the depth of the stress-fracturing or Depth Of Failure (DOF) zone in the observation cross-section. Fig. 8 shows the zone of the depth of stress-induced fracturing that was

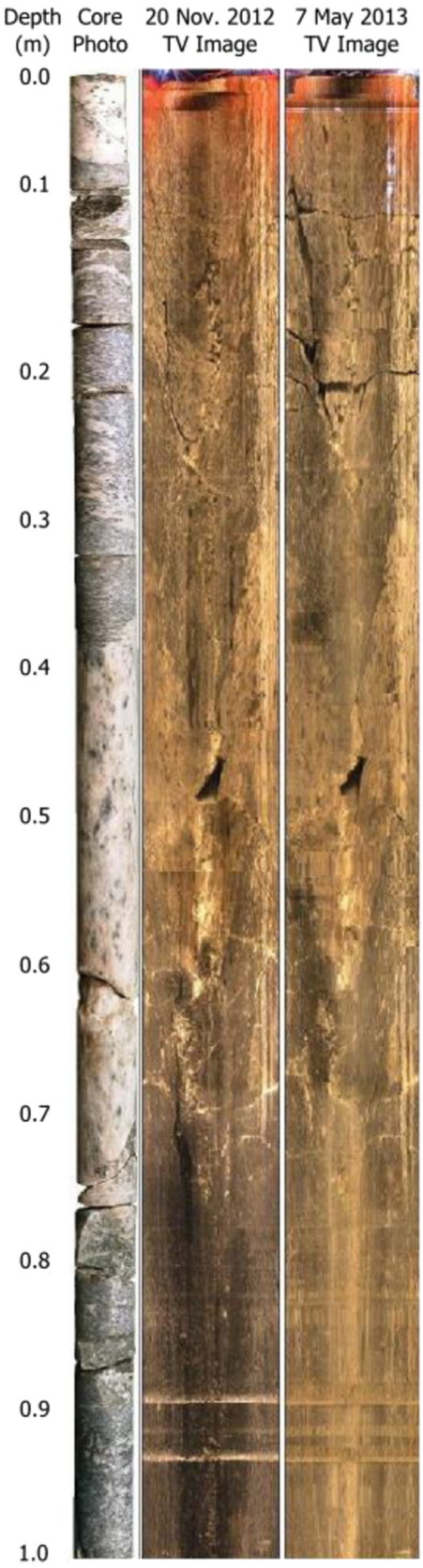

Fig. 7. Core and televiewer images from the first meter of Hole 3.

determined using the televiewer images. The safety bay was excavated between the first (Nov. 20, 2012) and the second (May 7, 2013) logging. Hole 11 was blocked and could not be logged by the

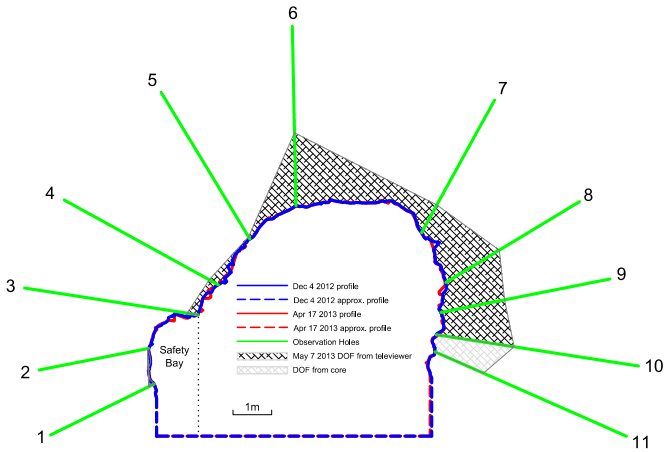

Fig. 8. Fractured zone mapped using core measurements and televiewer images logged on May 7th, 2013.

televiewer; hence, for this hole only the core was used to assess the depth of stress-induced fracturing. The depth of stress-induced fracturing varied drastically along the perimeter of the excavation, with most of the stress-induced fracturing concentrating in the zone that has been identified as being under the highest compressive stress. Measured depths of stress-induced fracturing in the high stress zone (Holes 6–11) ranged from 0.82 to 2.03 m.

It should be noted that Creighton Mine employs the practice of "destress blasting" to fracture the excavation wall at pre-determined locations in each 3.6 m development round. This procedure involves the detonation of 0.9 m of ammonium nitrate explosive at the end of each destress hole to pre-shear the rock mass ahead of each development round. Two holes on each wall are drilled looking out at 45°, one set at the shoulders looking up at 30° and another 0.6 m from the floor drilled flat. This places the end of each unconfined explosive charge at 2 m from the wall location, which is blasted as the first delay of the development round. The holes are washed and checked after each round prior to drilling and blasting. For the purpose of the project, the minimum distance to these charges based on frequent surveys is 1 m. The closest boreholes are #1 and #11 near the floor elevation and #5 and #7 in the shoulders (Fig. 3). No evidence of blast fracturing is evident, which was verified by high rock quality values obtained from core and direct observations by the televiewer images.

In practice, it is very difficult to determine U_w, because it is necessary to measure the wall deformation before excavation. Holes drilled from nearby pre-excavated excavations have been successfully used to monitor rock mass damage as the excavation under investigation was developed[15]; however, this technique is only possible when there is an appropriately located excavation available to drill the observation holes and is only capable of monitoring one side of the drift under investigation unless two or more suitably located excavations exist to allow more observation holes to be drilled before excavation of the opening under investigation. The observation holes at this site were drilled after the drift had been excavated, and a certain amount of deformation had already occurred before any measurements were made.

An alternative method used for this project was to measure U_w while processing the optical televiewer logs. The televiewer logs were processed using WellCAD, and the apertures of all open fractures were measured. If there is significant fracturing of the rock and many fractures are open, the sum of the apertures of all the fractures (both new and pre-existing fractures) intersecting a hole can be a good approximation of the convergence for the point at the collar of the hole. This is because before excavation, all pre-existing fractures in a rock mass at this depth are tightly closed

due to the confinement. Stress-induced fractures around an excavation tend to be approximately parallel to the surface of the excavation and the convergence is equal to the cumulative opening of such fractures [16]. Thus, it is not deemed necessary to correct for the orientation of the fractures relative to the orientation of the surface of the excavation. The sums of the apertures combined with the depths of failure measured in each hole allowed the bulking factor to be determined, even though no initial measurements had been made before the stress-induced damage from the excavation process occurred.

4.2. Ultrasonic velocity logging

It is well known that there is a strong correlation between the rock quality and wave velocity of the rock.[17–20] To study the link between the rock fracturing and wave velocity at the observation site, some of the observation holes were logged with an ultrasonic velocity probe. The probe consists of two transducers in contact with brass caps that slide along the wall of the hole. The transducers are attached to a bar that is floating on springs which ensures that firm contact is maintained between the brass caps and the wall of the hole. To improve the coupling between the brass caps and the wall of the hole, a coupling fluid (petroleum jelly) was pumped into the hole up to the bottom of the probe, coating the section of the hole that the brass caps were in contact with as the hole was logged.

It was found during logging that the S-wave was easier to pick and more reliable. P-wave signals emitted from the transmitter oscillate parallel to the direction of propagation, which is nearly perpendicular to the direction that the longitudinal wave transducer is able to detect motion. This results in the receiver receiving very weak signals and in some instances no signal at all. Alternatively, S-waves oscillate perpendicular to the direction of propagation, which is roughly parallel to the direction that the longitudinal wave transducer is able to detect motion, resulting in a signal that is easier for the receiver to pick up.

Fig. 9 presents the S-wave velocity (V_s) profile captured in Hole 3, with the televiewer image shown in the background. The S-wave velocity was relatively constant from the end of the hole to 1.25 m from the collar, ranging from 3100 to 3250 m/s, then from 1.25 to 0.85 m from the collar decreased to approximately 2600 m/s. From 0.85 m to the collar, the signal was attenuated to a point that no wave signals could be picked. The decrease in velocity from 1.25 to 0.85 m indicates that the rock was damaged; however, the absence of visible fractures in the televiewer image indicates that the rock was not failed. The attenuated signal from 0.85 m to the collar indicates that the rock was potentially fractured and under lower confinement. This is confirmed by the televiewer images shown in Fig. 7, which show stress-induced fracturing from the collar to a depth of 0.28 m and excavation-induced damage from 0.5 to 0.75 m. A decrease in confinement allows discontinuities of various scales to open up, resulting in a decrease in velocity[19]. Hence, without televiewer images the S-wave velocity profile would be interpreted as indicating a depth of failure of 0.85 m and a depth of damage of 1.25 m.

It can be concluded from this investigation that an ultrasonic velocity probe can be a useful tool for measuring the stress-fractured and stress-damaged zones. Logging from the deepest part of the hole towards the collar allows the operator to ensure the equipment is working properly and establish a baseline while the probe is in undamaged rock. In this case a decrease of the wave velocity and then a loss of the signal were seen as the probe approached the collar. The decrease in velocity is believed to be the result of micro fracturing of the rock, and the loss of signal is the result of macro fracturing of the rock and a decrease in confinement. Pairing velocity logging with an optical borehole logging method such as optical televiewer or borehole camera logging can aid in interpreting the results.

4.3. Logging friction sets using a borehole camera

The 2.7 M_n seismic event resulted in new fracturing within the rock mass and rock support damage in some of the scanned cross-sections, but not in the cross-section where the observation holes were drilled. In sections where rock fracturing was evident, the convergence was measured by rescanning the cross-sections with the laser scanner; however, without observation holes in these sections, the previously used techniques used to measure the depth of failure could not be used. Thus, a different approach was necessary to capture the depth of failure in these sections.

Forty six millimeter friction set bolts are typically used for wall support at Creighton Mine. There is a slot in each bolt, which coincidentally provides a convenient channel for observation of the rock mass condition directly. A small diameter borehole camera was inserted into a few bolts at the area of interest, i.e., the wall section with the greatest convergence. The information collected was used to determine the depth of fracturing. The investigation revealed that friction sets were pinched by a shearing action that occurred along a major fracture with a substantial aperture. Previous observations at Creighton mine have shown that this is not an uncommon form of damage to split sets that are retaining bulked ground resulting from a seismic event.[21] Measurements taken in other friction sets that intersected the same fracture but were not completely pinched showed no additional stress fracturing beyond this point. On this basis, the points at which the bolts were pinched were considered to be the extent of the stress-induced fracturing. Fig. 10a,b show the measured depths of stress fracturing and laser scans in cross-sections CS5 and CS6, respectively. The upper bolt measurement shown in Fig. 10a is an interpolation of two measurements that were taken from two bolts. Both bolts were situated at the same height, the first 20 cm to one side of CS5 and the other 30 cm on the opposite side of CS5. The depths of stress-induced fracturing measured in both friction sets were almost identical.

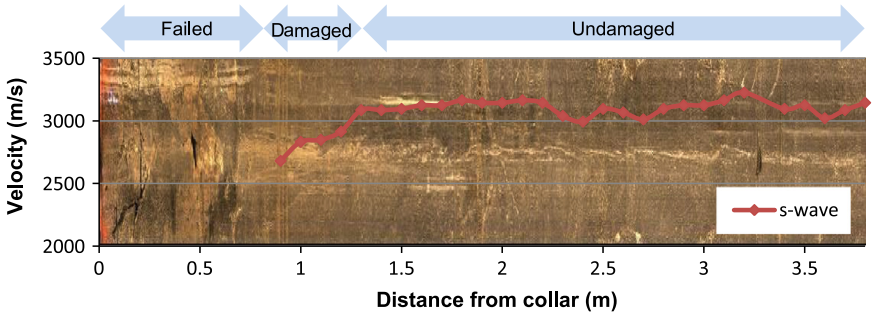

Fig. 9. V_s profile from Hole 3 with the televiewer image in the background.

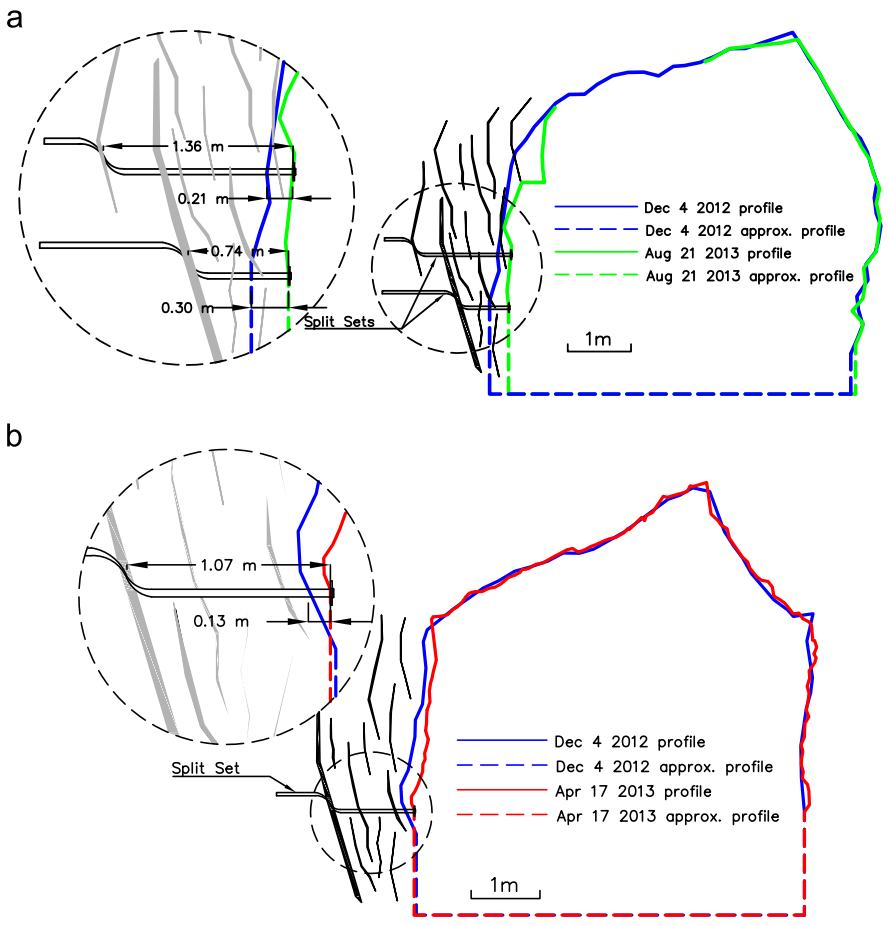

Fig. 10. Depth of stress fracturing measured in friction sets (Split sets) in (a) Cross-section 5, and (b) Cross-section 6.

This investigation demonstrates that observing the rock mass condition through the installed friction sets can provide useful information for assessing the depth of rock fracturing in the rock mass. No costly diamond boreholes are needed and the borehole camera is also less expensive than the optical televiewer.

5. Discussion

5.1. Performance of rock support

Fig. 11 presents some of the damage to friction sets and the surrounding rock mass as a result of the 2.7 M_n seismic event which resulted in fracturing along the wall near the cut-out location. Fig. 11a and b show parallel spalling fractures that are aligned with the drift wall. Fig. 11b and c reveal that the 46 mm friction sets accommodated a significant amount of deformation while at the same time continued to support the fractured rocks. In Fig. 11c, the friction set appeared to have been subjected to downward shearing, implying that the block may have slid downwards before moving further into the excavation. Pull-out strengths for this type of bolt in footwall rocks are in the range of 8.5–9.5 t. As the rock mass fractures and the bolts lock-in due to shearing, increases in pull-out strengths to 11–12 t is not uncommon.

Fig. 11d captures a friction set which appears to have failed in tension. Less common of an occurrence at Creighton Mine, the bolt might have failed at 18–19 t, which is the approximate measured tensile strength of the tube and welded ring. It is suspected that the bolt may have locked-up internally with the movement of the ground motion and exceeded its load capacity. A qualitative assessment of the demand on the support system reveals the anticipated level of ground motion under typical conditions is high (>0.1 m/s peak particle velocity) for a magnitude 2.7 M_n event 45 m from the damage location and that the damage mechanism falls within the rock bulking category. This corresponds to greater than 5 MPa of maximum dynamic stress induced at the wall of the excavation.[2] These examples illustrate that the friction sets worked effectively by deforming and absorbing the energy imparted on the rock mass near the surface of the excavation, with sufficient remaining capacity to retain the failed rocks.

5.2. Bulking factors from televiewer data

The depth of failure and convergence measurements collected from the observation holes can be used to calculate the associated bulking factors. The levels of confinement applied to the walls and the back were calculated based on the support type and pattern utilized. The support in the wall consists of friction sets and welded wire mesh, and the support in the back consists of modified conebolts (MCB33[3,22]), rebars, and welded wire mesh. Measurements made in the walls and the back are grouped as such, and the average and range of values are used for displaying the data.

Fig. 12 presents the average and the range of bulking factors in the back and walls from this study (red symbols), together with some field data summarized in[5], and data obtained from numerical modeling using ELFEN[23]. The bulking factors, calculated based on the measured wall deformation and depths of failure at each observation hole, ranged from 1.4% to 6.6% in the wall and 1.6% to 2.7% in the back. The bulking factors from this study are lower

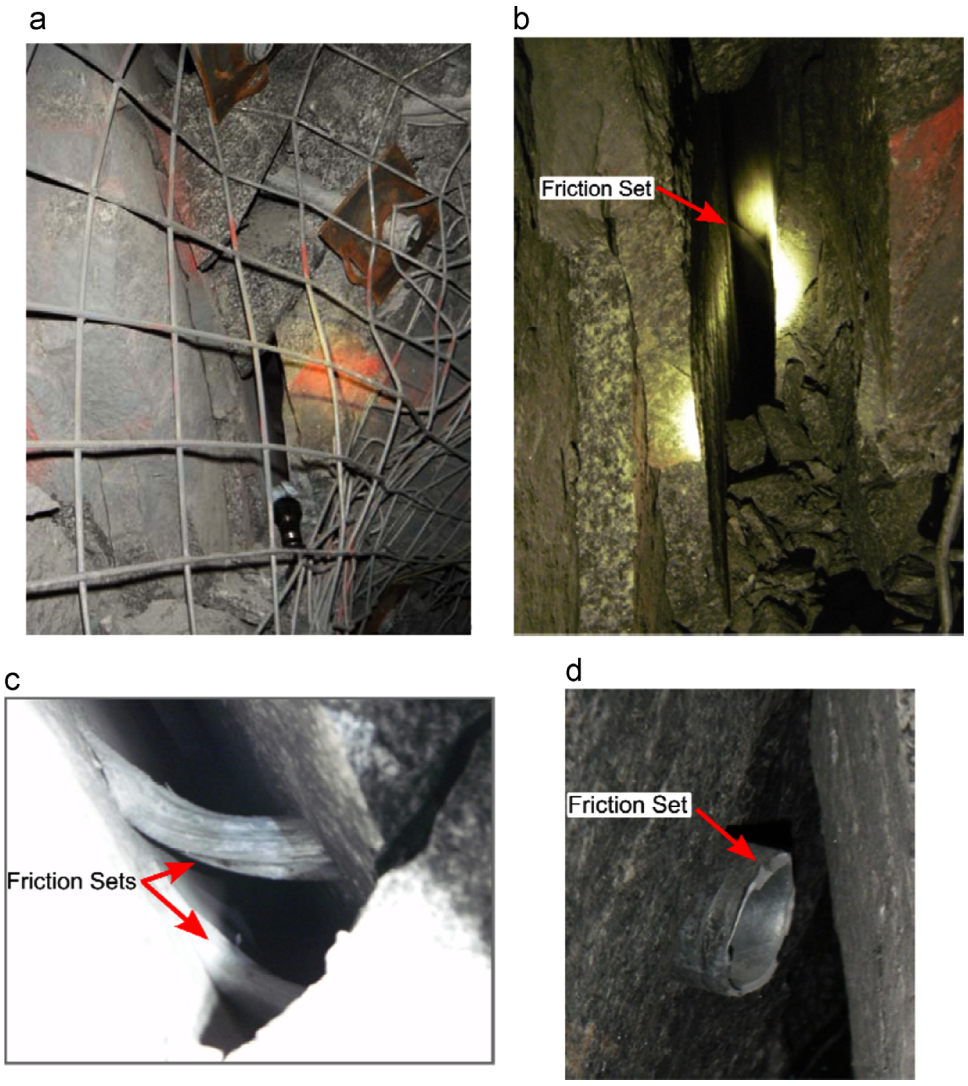

Fig. 11. Damage to friction sets and rock mass in the wall adjacent to the safety bay as a result of the 2.7 M_n seismic event.

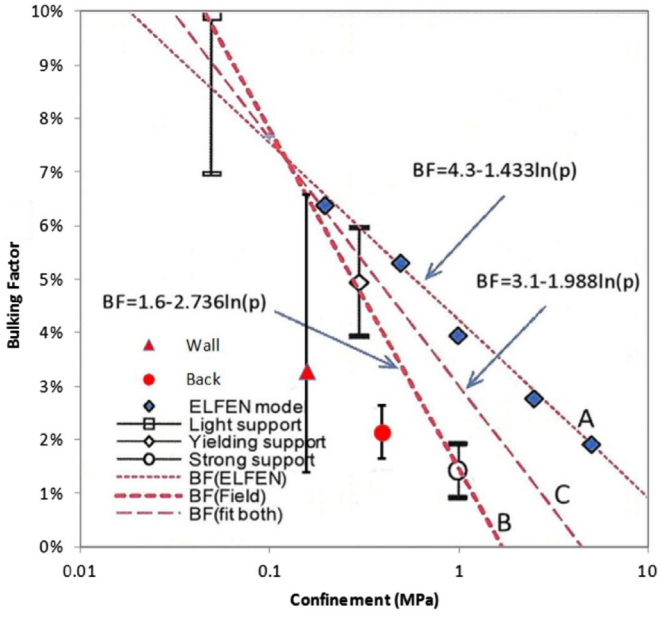

Fig. 12. Bulking factors plotted on a graph modified from Ref. 4. (For interpretation of the references to color in this figure legend, the reader is referred to the web version of this article.)

than those from previous studies. This is expected because the data from previous studies corresponded to cases in which severe damage to the rock mass and rock support system had occurred. The numerical simulation in[23] considered complete failure of rock with sufficient straining under different confinements. On the other hand, the degree of damage to the rock mass and support in this case study was minor. Based on the rock support damage scale suggested in Ref. 2, the damage level for the rock support alongside the observation holes is S1, meaning that it is undamaged but loaded. Therefore, the resulting bulking factors were small. In other words, if the installed rock support system is effective in controlling the rockburst damage, the amount of wall deformation can be limited and the corresponding bulking factors can be less than that in excavations with ineffective rock support.

5.3. *Relative bulking factors from friction set measurements*

In Cross-sections 5 and 6 (CS5 and CS6), where the depth of failure was measured by inserting a borehole camera into friction sets, the total wall deformation (U_w) is not known. This is because when the initial scanned cross-sections were captured, it was likely that some stress-induced fracturing, and consequently convergence had already occurred. Unlike the optical televiewer, the borehole camera does not allow the aperture of fractures to be

measured so as to estimate the wall convergence. The convergence values shown in Fig. 10 are relative to the first scan that was performed, and any bulking factors calculated using these values would be as well. This will be referred to as the relative bulking factor (BF'), calculated using Eq. (3). BF' will always be equal to or less than BF, depending whether convergence has occurred prior to the initial measurement:

$$BF' = \Delta U_w \times d_f \quad (3)$$

In CS5 in the upper friction set, the deformation was 0.21 m and the depth of failure was 1.36 m, which gave a BF′ of 15%; and in the lower friction set the deformation was 0.30 m and the depth of failure was 0.74 m, which gave a BF' of 41%. In CS6 the deformation was 0.13 m and the depth of failure was 1.07 m, which gave a BF' of 12%. At this location, the depths of failure are relatively small but the relative bulking factors are exceptionally large; hence, the resulting maximum wall deformation was up to 0.30 m.

The values of BF' are higher than the 10% bulking factor that would typically be recommended for this situation. The large values of 12% and 15% are a result of the large open fracture shown in Fig. 11a and b. The seismic event that caused the rock mass bulking likely imparted a velocity onto the fractured mass of rock and the friction sets deformed to absorb the energy of the fractured zone, resulting in a large open fracture. The location where the relative bulking factor was 41% may be the result of a combination of the deformation being large due to geometric incompatibility caused by the movement of a single large block and the depth of stress-induced fracturing being relatively small.

6. Conclusions

This paper presents a case study conducted at a deep drift in Creighton Mine in Canada where quantitative measurements pertaining to rock mass bulking were made using a variety of techniques. The main insights gained from this study are as follows:

(1) Bulking factors at the location where the observation holes were drilled ranged from 1.4% to 6.6% where the support was loaded but undamaged. This means that if the rock support system is effective in controlling rockburst damage, the resulting rock mass deformation can be small. This is important because by limiting the wall deformation rehabilitation can be avoided after a major rockburst event. For this reason, rockburst resistant rock support systems should be used in highly stressed grounds.

(2) Large relative bulking factors ranging from 12% to 41% were observed locally in a section of the drift wall that was damaged by the seismic event. The larger than expected relative bulking factors are local and are mostly the result of a geometric incompatibility caused by the movement of a single large block. In other words, large bulking factors beyond what is typically expected are possible if there is block rotation and shear movement between blocks involved.

(3) Logging diamond drilled holes with an optical televiewer proved to be the most useful technique for monitoring the depth of failure for rock mass bulking assessment. Other data collection techniques such as core logging, ultrasonic velocity logging, laser scanning, and borehole camera logging in friction sets have their own merits and added value to the overall description and monitoring of the site. If there is core disking in the core samples, the depth of stress-induced fracturing in holes perpendicular to the maximum tangential stress can be estimated based on the location of core disking from the collar. The S-wave velocity profile from the ultrasonic velocity probe can be used to estimate the depth of failure and the depth of micro fracturing. When drilled observation holes are not available, borehole cameras can be used to observe rock mass damage status in friction sets. However, this may be restricted by availability of accessible bolts installed in the walls.

As mining continues at the deep levels of Creighton Mine, additional stress changes will occur and further deformation of the rock mass at the observation site is expected. Creighton Mine geotechnical staff and Laurentian University researchers plan to periodically visit the observation site and monitor the evolution of wall deformation and depth of rock fracturing. New results and insights will be made available in future publications.

Acknowledgments

Financial support from CEMI, Vale, LKAB, and NSERC as well as in kind support from Vale and MIRARCO are gratefully acknowledged. The authors appreciate the help of many people on this project including the geotechnical staff from Creighton Mine, and the staff and students from the Geomechanics Research Center at MIRARCO. In particular, the authors are grateful to Denis Thibodeau for helping to initiate the project and arranging the field work at Creighton Mine; Byron Seguin, Jim Duncan, and Natalie Kari for their help with logistics at Creighton Mine; Don Chartrand, Brian Langlois, and Bob Pelkey for their help with the drilling and retrieval of the cores; Samantha Espley and Mike Yao for approving the publication of the work; Damien Duff for promoting the project; Peter Kaiser for his prominent publications on the topic; and Sean Maloney for his advice on field and lab equipment.

References

1. Cai M, Kaiser PK, Duff D. Rock support design in burst-prone ground utilizing an interactive design tool. In: *Proceedings of the 46th US Rock Mechanics Symposium 2012, Paper ARMA* 12-599; 2012.
2. Kaiser PK, Tannant DD, McCreath DR. *Canadian Rockburst Support Handbook.* Sudbury, Ontario: Geomechanics Research Centre, Laurentian University; 1996.
3. Cai M, Champaigne D, Kaiser PK. Development of a fully debonded conebolt for rockburst support. In: Van Sint Jan M, Potvin Y, eds. *Proceedings of the 5th International Seminar on Deep and High Stress Mining*; 2010:329–342.
4. Cai M, Kaiser PK. A Guide to Rockburst Support Selection, 2015, Geomechanics Research Centre, Laurentian University, Sudbury, Ontario.
5. Kaiser PK. Rock mechanics considerations for construction of deep tunnels in brittle rock. In: Leung CF, Zhou YX, eds. *Proceedings of the 4th Asian Rock Mechanics Symposium*; 2006:47–58.
6. Sevume C. In situ instrumentation and monitoring of the deformation of a tunnel in a highly stressed hard rock mass. In: *Proceedings of the 9th International Congress Rock Mechanics, Sandton, SA*; 1999:1429–1434.
7. Pelli F, Kaiser PK, Morgenstern NR. An interpretation of ground movements recorded during construction of the Donkin–Morien tunnel. *Can Geotech J.* 1991;28(2)239–254.
8. Malek F, Suorineni F, Vasak P. Geomechanics strategies for rockburst management at Vale Inco Creighton Mine. In: Diederichs M, Grasselli G, eds. *Proceedings 3rd Canada–US Rock Mechanics Symposium*. Paper 4234; 2009.
9. Barton NR, Lien R, Lunde J. Engineering classification of rock masses for the design of tunnel support. *Rock Mech.* 1974;6(4)189–239.
10. Hoek E, Kaiser PK, Bawden WF. *Support of Underground Excavations in Hard Rock.* Rotterdam: Balkema; 1995.
11. Martin CD, Stimpson B. The effect of sample disturbance on laboratory properties of Lac du Bonnet granite. *Can Geotech J.* 1994;31:692–702.
12. Lim SS, Martin CD. Core disking and its relationship with stress magnitude for Lac du Bonnet granite. *Int J Rock Mech Min Sci.* 2010;47(2)254–264.
13. Schmitt DR, Currie CA, Zhang L. Crustal stress determination from boreholes and rock cores: fundamental principles. *Tectonophysics.* 2012;580:1–26.
14. Martin CD, Kaiser PK, McCreath DR. Hoek–Brown parameters for predicting the depth of brittle failure around tunnels. *Can Geotech J.* 1999;36(1)136–151.
15. Uchida Y, Harada T, Kanagawa T, Nakagawa K, Urayama M, Nakamura T, Ishida T. Mechanical rock behavior of cavern wall during underground powerhouse

excavation. In: *Proceedings of the 24th Japan Symposium on Rock Mechanics JSCE*; 1997:316–320.
16. Cai M. Influence of intermediate principal stress on rock fracturing and strength near excavation boundaries-insight from numerical modeling. *Int J Rock Mech Min Sci.* 2008;45(5)763–772.
17. Young RP, Collins DS. Monitoring an experimental tunnel seal in granite using acoustic emission and ultrasonic velocity. In: *Proceedings of the 37th US Rock Mechanics Symposium*. Balkema; 1999:869–876.
18. Barton N. Some new Q-value correlations to assist in site characterisation and tunnel design. *Int J Rock Mech Min Sci.* 2002;39(2)185–216.
19. Cai M, Kaiser PK. Dependency of wave propagation velocity on rock mass quality and confinement. In: Hammah R, Bawden W, Curran J, Telesnicki M, editors. *NARMS 2002.* Toronto, Ont.: University of Toronto Press; 2002. p. 615–622.
20. Cai M, Kaiser PK. Assessment of excavation damaged zone using micro-mechanics model. *Tunn Undergr Space Technol.* 2005;20(4)301–310.
21. Punkkinen A, Yao M. Change of ground support system and mining practice in the deep at Creighton Mine. In: *Proceedings of CIM 2007*; 2007.
22. Cai M, Champaigne D. Influence of bolt-grout bonding on MCB conebolt performance. *Int J Rock Mech Min Sci.* 2012;49(1)165–175.
23. Cai M. *Resolution rock support scoping study – support design and selection rationale.* Sudbury, Ontario: Geomechanics Research Centre, Laurentian University; 2006.